Self-shading correction for upwelling sea-surface radiance measurements made with buoyed instruments

Robert A. Leathers, T. Valerie Downes

Naval Research Laboratory, Code 7212
4555 Overlook Ave. SW, Washington, DC 20375
leathers@rsd.nrl.navy.mil, downes@rsd.nrl.navy.mil
http://rsd-www.nrl.navy.mil/7212/

Curtis D. Mobley

Sequoia Scientific, Inc.
15317 NE 90th Street, Redmond, WA 98052
mobley@sequoiasci.com

Abstract: Upwelling radiance measurements made with instruments designed to float at the sea surface are shaded both by the instrument housing and by the buoy that holds the instrument. The amount of shading is wavelength dependent and is affected by the local marine and atmospheric conditions. Radiance measurements made with such instruments should be corrected for this self-shading error before being applied to remote sensing calibrations or remote sensing algorithm validation. Here we use Monte Carlo simulations to compute the self-shading error of a commercially available buoyed radiometer so that measurements made with this instrument can be improved. This approach can be easily adapted to the dimensions of other instruments.

OCIS codes: (010.4450) Ocean Optics; (290.4210) Multiple Scattering

References and links

1. H. R. Gordon and K. Ding, "Self-shading of in-water optical instruments," Limnol. Oceanogr. **37**, 491–500 (1992).
2. D. R. Lyzenga, "Remote sensing of bottom reflectance and water attenuation parameters in shallow water using aircraft and Landsat data," Int. J. Remote Sensing **2**, 71–82 (1981).
3. H. R. Gordon, O. B. Brown, R. H. Evans, J. W. Brown, R. C. Smith, K. S. Baker, and D. K. Clark, "A semianalytic radiance model of ocean color," J. Geophys. Res. **93**, 10909–10924 (1988).
4. J. E. O'Reilley, S. Maritorena, B. G. Mitchell, D. A. Siegel, K. L. Carder, S. A. Garver, M. Kahru, and C. McClain, "Ocean color chlorophyll algorithms for SeaWiFS," J. Geophys. Res. **103**, 24937-24953 (1998).
5. D. R. Lyzenga, "Passive remote sensing techniques for mapping water depth and bottom features," Appl. Opt. **17**, 379–383 (1978).
6. G. Zibordi and G. M. Ferrari, "Instrument self-shading in underwater optical measurements: experimental data," Appl. Opt. **34**, 2750–2754 (1995).
7. E. Aas and B. Korsbø, "Self-shading effect by radiance meters on upward radiance observed in coastal waters," Limnol. Oceanogr. **42**, 968–974 (1997).
8. J. Piskozub, A. R. Weeks, J. N. Schwarz, and I. S. Robinson, "Self-shading of upwelling irradiance for an instrument with sensors on a sidearm," Appl. Opt. **39**, 1872–1878 (2000).
9. G. S. Fargion and J. L. Mueller, *Ocean optics protocols for satellite ocean color sensor validation, revision 2* (NASA Tech. Memo. 209966, NASA Goddard Space Flight Center, Greenbelt, Maryland, 2000).
10. Coastal Benthic Optical Properties, http://www.psicorp.com/cobop/cobop.html.

#32933 - $15.00 US
Received April 17, 2001; Revised May 01, 2001

11. H. R. Gordon, "Ship perturbation of irradiance measurements at sea. 1. Monte-Carlo simulations," Appl. Opt. **24**, 4172–4182 (1985).
12. C. D. Mobley, *Light and Water. Radiative Transfer in Natural Waters*, (Academic Press, New York, 1994).
13. G. R. Fournier and J. L. Forand, "Analytic phase function for ocean water," in *Ocean Optics XII*, J. S. Jaffe, ed., Proc. SPIE 2258, 194–201 (1994).
14. C. D. Mobley, B. Gentili, H. R. Gordon, Z. Jin, G. W. Kattawar, A. Morel, P. Reinersman, K. Stamnes, and R. H. Stavn, "Comparison of numerical models for computing underwater light fields," Appl. Opt. **32**, 7484–7504 (1993).
15. C. Cox and W. Munk, "Statistics of the sea surface derived from sun glitter," J. Mar. Res. **13**, 198–227 (1954).
16. S. McLean, Satlantic Incorporated, Halifax, Nova Scotia, Canada. Personal correspondence.
17. A. Ariew, "Are probabilities necessary for evolutionary explanations?," Biol. Phil. **13**, 245-253 (1998).
18. A. W. Harrison and C. A. Coombes, "An opaque cloud cover model of sky short wavelength radiance," Solar Energy **41**, 387–392 (1988).
19. C. S. Roesler, "Theoretical and experimental approaches to improve the accuracy of particulate absorption coefficients derived from the quantitative filter technique," Limnol. Oceanogr. **43**, 1649-1660 (1998).
20. R. A. Leathers, T. V. Downes, and C. O. Davis, "Analysis of a point-source integrating-cavity absorption meter," Appl. Opt. **39**, 6118–6127 (2000).
21. L. Prieur and S. Sathyendranath, "An optical classification of coastal and oceanic waters based on the specific spectral absorption curves of phytoplankton pigments, dissolved organic matter, and other particulate materials," Limnol. Oceanogr. **26**, 671–689 (1981).
22. R. M. Pope and E. S. Fry, "Absorption spectrum (380–700nm) of pure water. II. Integrating cavity measurements," Appl. Opt. **36** 8710–8723, (1997).
23. R. C. Smith and K. S. Baker, "Optical properties of the clearest natural waters (200-800 nm)," Appl. Opt. **20**, 177–184 (1981).
24. W. W. Gregg and K. L. Carder, "A simple spectral solar irradiance model for cloudless maritime atmospheres," Limnol. Oceanogr. **35** 1657–1675, (1990).
25. H. R. Gordon, "Dependence of the diffuse reflectance of natural waters on the sun angle," Limnol. Oceanogr. **34**, 1484–1489 (1989).
26. K. S. Baker and R. C. Smith, "Irradiance transmittance through the air-water interface," in *Ocean Optics X*, R. W. Spinrad, ed., Proc. SPIE 1302, 556–565 (1990).

1 Introduction

When an instrument is placed in water to measure the upwelling light, the magnitude of the local light field is decreased by the shadow of the instrument. This effect can be large in turbid waters [1], causing several practical problems. Vicarious calibrations of remote sensing radiometers will be in error when performed with shaded in-water radiance measurements, and remote-sensing reflectance values will be underestimated when calculated from shaded upwelling radiance measurements and unshaded downwelling irradiance measurements. Furthermore, because the magnitude of the shading error is wavelength dependent, algorithms that depend on ratios of the radiance at different wavelengths to determine water optical properties [2], water constituent concentrations [3, 4], or bottom depth or features [5] will also be in error. Therefore, shading corrections should be routinely applied to upwelling light measurements. The self-shading of in-water instruments has been investigated by Gordon and Ding [1], Zibordi and Ferrari [6], Aas and Korsbø [7], and Piskozub, Weeks, Schwarz, and Robinson [8].

Gordon and Ding [1] provide a semianalytical model for the self-shading error of sea-surface upwelling radiance and irradiance measurements in optically deep waters. The ocean optics protocols for SeaWiFS validation [9] recommends the use of this model, and Zibordi and Ferrari [6] found good agreement between the model and their experimental estimates of self-shading. The fractional error in this model is predicted with

$$\varepsilon = [1 - \exp(-kar)], \tag{1}$$

#32933 - $15.00 US Received April 17, 2001; Revised May 01, 2001

where a is the water beam absorption coefficient, r is the radius of the instrument housing, and k is a constant that depends on the measurement type and on the illumination conditions. Gordon and Ding [1] derived values of k with Monte Carlo simulations of a two-dimensional shading disk placed just below the sea surface. For radiance measurements and a sun in a black sky, $k \approx 2/\tan\theta_{0w}$, where θ_{0w} is the in-water solar zenith angle. The shading error for general sky conditions can be approximated with [1, 6]

$$\varepsilon = \frac{\varepsilon_{\text{sun}} + \varepsilon_{\text{sky}} f}{1 + f}, \tag{2}$$

where ε_{sun} is the shading error for direct sunlight from the appropriate sun angle, ε_{sky} is the shading error for skylight, and f is ratio of the downwelling irradiance from skylight to that from direct sunlight.

Unfortunately, for upwelling light sensors mounted in instruments that use a buoy to float on the sea surface, Eq. (1) is inappropriate. Because the buoy has a larger radius than the sensor housing and is vertically separated from the sensor depth, it could be expected that the actual shading of the instrument in optically deep water is greater than that predicted by Eq. (1) for the sensor housing alone but less than that predicted by Eq. (1) for the buoy. Equation (1) is also not valid for optically shallow waters, in which the shading error is highly dependent on water depth and the seafloor characteristics.

Here we use Monte Carlo simulations to quantify the shading effects of cylindrical instruments and the additional shading of a wider cylindrical surface buoy. Our specific objective is to derive a shading correction algorithm for the Hyper-TSRB (Satlantic Inc., Halifax, Nova Scotia, Canada), which was extensively used in recent CoBOP [10] experiments for *in situ* studies and as sea-truth for aircraft remote sensing systems. The approach demonstrated here and most of our qualitative conclusions apply to any set of instrument dimensions; only the quantitative results are specific to the TSRB.

2 Methods

Simulated responses of an upwelling radiance detector with and without the presence of a shading object were computed using Backward Monte Carlo (BMC) ray tracing as described in Ref. 11. In BMC codes simulated photons are emitted from the sensor and traced backwards to the light source. For geometries involving an extended source (the sky in our case) and small sensor (as on the TSRB), the BMC technique is numerically efficient because every traced photon contributes to the statistical estimate of the upwelling radiance at the instrument. The radiance sensor is treated as a point sensor located at the bottom center of a cylindrical casing. After emission from the sensor, the photons are traced using standard techniques for forward Monte Carlo ocean optics simulations as described in Ref. 12. Shading is simulated by removing any photon whose path intersects the cylinder. The equations necessary to check for photon-cylinder intersections in a Monte Carlo algorithm are given later in this section. In our BMC code the effects of the illumination conditions are applied last, allowing us to apply many different sky conditions to the same in-water ray-tracing results. For most computations we used the Fournier-Forand [13] scattering phase function with the parameters chosen to closely match the Petzold particle [14] scattering phase function. The seafloor was assumed to be Lambertian with a given irradiance reflectance, and the shape of the sea surface was taken to be that of capillary waves as described by Cox-Munk statistics [15].

The TSRB was modeled as two cylinders extending into the water from the sea surface. The main body has a 4.4 cm radius and extends 66 cm into the water, whereas the buoy has a 15 cm radius and extends 12 cm into the water. Potential shading due to the portion of the TSRB that is above the waterline was not included, but we expect

#32933 - $15.00 US Received April 17, 2001; Revised May 01, 2001

this to be insignificant for upwelling radiance measurements. The TSRB radiance sensor response characteristics were modeled from measurements provided by Satlantic [16].

The shading error ε was computed for each set of water properties and illumination conditions with

$$\varepsilon = (L_u^{\text{true}} - L_u^{\text{m}})/L_u^{\text{true}}, \tag{3}$$

where L_u^{m} is the simulated sensor response with shading and L_u^{true} is the simulated unshaded sensor response. Many runs of the Monte Carlo code were made for each case but with different seeds of the random number generator so that the statistical uncertainty [17] of the simulations could be estimated.

The parametric equation for the line segment describing a photon path is

$$\begin{bmatrix} x \\ y \\ z \end{bmatrix} = \begin{bmatrix} x_1 \\ y_1 \\ z_1 \end{bmatrix} + \begin{bmatrix} \alpha \\ \beta \\ \gamma \end{bmatrix} s, \qquad 0 \le s \le L, \tag{4}$$

where x and y are horizontal positions, z is depth (m), (x_1, y_1, z_1) is the starting point of the line segment, α, β, and γ are the direction cosines of the line segment, and L is the length of the line segment (i.e., the distance the photon travels). The parametric equation for the solid cylinder describing the instrument is

$$\begin{bmatrix} x \\ y \\ z \end{bmatrix} = \begin{bmatrix} x_0 \\ y_0 \\ z_0 \end{bmatrix} + \begin{bmatrix} \rho\cos(\theta) \\ \rho\sin(\theta) \\ u \end{bmatrix}, \qquad \begin{matrix} 0 \le \rho \le r \\ 0 \le \theta \le 2\pi, \\ 0 \le u \le h, \end{matrix} \tag{5}$$

where (x_0, y_0, z_0) is the location of the bottom center of the cylinder and r and h are the cylinder radius and height. The intersection points between the line coincident with the photon path and an infinite cylinder coincident with the cylinder wall satisfy

$$(x_1 - x_0 + \alpha s)^2 + (y_1 - y_0 + \beta s)^2 = r^2. \tag{6}$$

$$\tag{7}$$

Equation (6) is quadratic in s, the solutions of which are

$$s = \frac{-B \pm \sqrt{B^2 - 4AC}}{2A}, \qquad \begin{matrix} A = \alpha^2 + \beta^2, \\ B = 2\alpha(x1 - x0) + 2\beta(y1 - y0), \\ C = (x1 - x0)^2 + (y1 - y0)^2 - r^2. \end{matrix} \tag{8}$$

There are no intersection points if $(B^2 - 4AC) < 0$. Otherwise, for solutions s_1 and s_2, the range of values of s for which the infinite line intersects an infinitely tall solid cylinder is $s_1 \le s \le s_2$. The finite photon path (of length L) is a subsegment of this infinite line. Values of s that satisfy $s \in [\max(0, s) \le s \le \min(L, s_2)]$ define the portion of the photon path that intersects the infinitely tall solid cylinder. If this range of s is finite, we find the boundaries of the corresponding range of u by substituting the limits of s into [from Eqs. (4) and (5)]

$$u = z_1 - z_0 + \gamma s. \tag{9}$$

If this range of u overlaps $0 \le u \le h$ at any point, then the photon is known to hit the cylinder of height h.

3 Results

Figure 1 shows the TSRB self-shading error in optically deep water versus the water beam absorption coefficient a (m^{-1}) compared with the errors predicted by Eqs. (1)

#32933 - $15.00 US Received April 17, 2001; Revised May 01, 2001

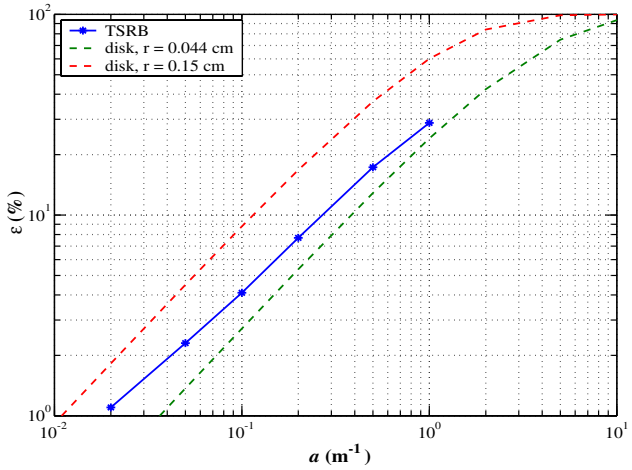

Fig. 1. Self-shading error of the TSRB (solid line) in deep water for $b/a = 2$ compared with that computed with Eqs. (1) and (2) for radii 0.044 m and 0.15 m. The TSRB error was computed for an empirical sky model at 480 nm with the sun zenith angle $\theta_0 = 30$ degrees.

and (2) for shading disks with radii of the TSRB instrument body and TSRB buoy, respectively. As expected, the shading error of the TSRB is larger than that of a disk with $r = 0.044$ m (the TSRB body radius) because of the presence of the buoy, but is less than that of a disk with $r = 0.15$ m (the buoy radius) because there is vertical separation between the buoy and the sensor. Because the optical distance between the buoy and the sensor is larger in turbid waters than in clear waters, the TSRB shading error in turbid water is closer to that of a disk with the instrument radius than that of a disk with the buoy radius and vice versa in clear waters.

Figure 2 shows the shading error versus a for optically deep water, $b/a = 2$, and five solar zenith angles θ_0 for a sun in a black sky. For large values of θ_0 the error increases approximately linearly with a for $0.02 < a < 1$, whereas for smaller sun angle, and therefore larger shading errors, the error depends on a in a nonlinear manner. Equation (1) gives a poor fit to the curves in Fig. 2, either underestimating the error at low values of a or overestimating the error at high values of a, depending on the chosen value of k.

As shown in Fig. 2, self-shading error depends strongly on sun position. The top plot in Fig. 3 shows the upwelling radiance L_u versus solar zenith angle both when the TSRB is present and in its absence. These simulations are for a sun in a black sky, optically deep water, and $a = b = 0.2$ m^{-1}. The values of L_u shown in Fig. 3 are normalized by the downward irradiance at the sea surface $E_d(0)$. The shading error, shown in the bottom plot of Fig. 3, is large for small sun angles and small for large sun angles. Here, too, we see that the TSRB shading error in deep water lies between those predicted by Eq. (1) for the two TSRB radii. Also shown in Fig. 3 is the error due to the main body of the TSRB without the buoy. It can be seen that the buoy has a large effect, but only for $\theta_0 < 20°$. This was found to be true in general, and therefore the shading error of the TSRB has a much stronger dependence on θ_0 than does that of a non-buoyed cylindrical instrument. Figure 4 shows the TSRB shading error versus solar zenith angle for a sun in a black sky, six values of a, and $b = 2a$. For all values of a, the shading error is significant at small values of θ_0 and decreases with increasing θ_0.

For a given value of a the shading error in optically deep water is generally smallest for large values of b because scattering enables the regions shadowed from direct light

#32933 - $15.00 US
Received April 17, 2001; Revised May 01, 2001

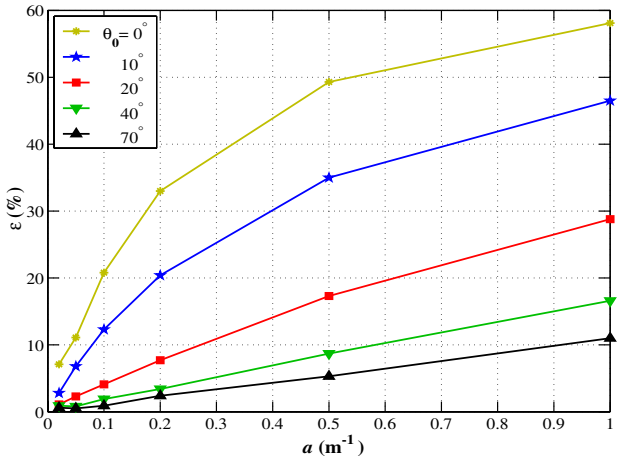

Fig. 2. Self-shading error of the TSRB in deep water for $b/a = 2$, five solar zenith angles, and no skylight.

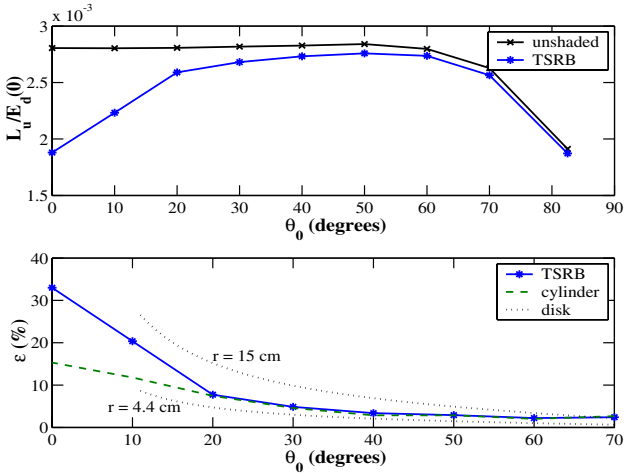

Fig. 3. Shaded and unshaded normalized radiance and percent shading error of the TSRB and of the TSRB cylindrical body without the buoy compared with Eq. (1) for radii 0.044 m and 0.15 m. The computations are for a sun in a black sky, deep water, and $a = b = 0.2$ m^{-1}.

#32933 - $15.00 US
Received April 17, 2001; Revised May 01, 2001

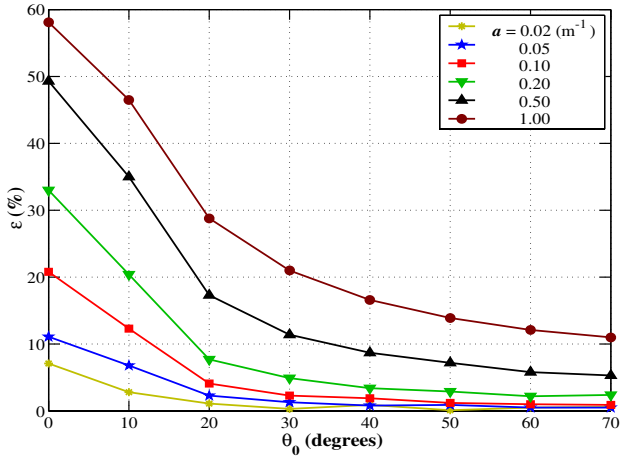

Fig. 4. Percent shading error of the TSRB in deep water versus solar zenith angle θ_0 for a sun in a black sky, six values of a, and $b/a = 2$.

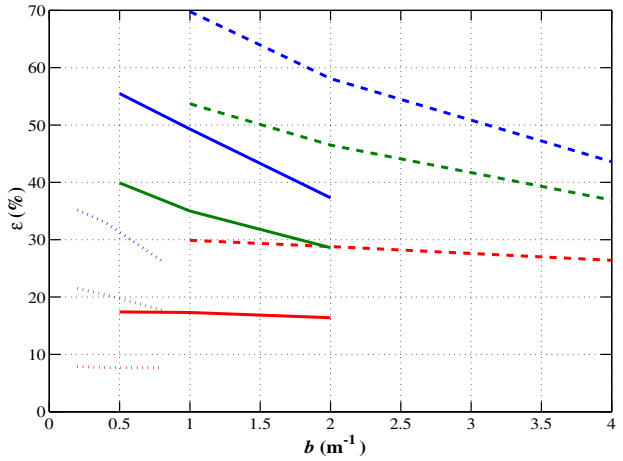

Fig. 5. Percent shading error of the TSRB in deep water for a =0.02 m^{-1} (dashed), 0.05 m^{-1} (solid), and 1.0 m^{-1} (dotted) and $\theta_0 = 0°$ (top, blue), 10° (middle, green), and 20° (bottom, red).

to be filled in with scattered light. However, we found this effect to be significant only for small values of θ_0, where the shading effect is greatest. Shown in Fig. 5 is the TSRB shading error versus b for $\theta_0 = 0$, 10, and 20 degrees, each for $a = 0.2$, 0.5, and 1.0 m^{-1}. It can be seen that the slope of shading error curves are similar for constant θ_0 but that this slope decreases with increasing θ_0.

Table 1 lists the TSRB shading error for flat, optically deep water both for a diffuse sky and for a sun in a black sky at eight solar zenith angles. Results are shown for six values of a and, for $\theta_0 \leq 20°$, three values of b/a. For $\theta_0 > 20°$ the dependence on b was found to be insignificant and the results shown in Table 1 are those for $b/a = 1$, 2, and 4 averaged together. Estimates of the statistical uncertainty in the error values, derived from the standard deviation of the simulations, is provided for the smallest and largest values of a.

Wind-induced surface capillary waves tend to spread out the angular distribution of incoming light. This can reduce the shading error when the sun is high in the sky by

#32933 - $15.00 US
Received April 17, 2001; Revised May 01, 2001

Table 1. Percent shading error ($100\times\varepsilon$) of a TSRB for given values of absorption coefficient a, scattering coefficient b, and solar zenith angle θ_0.

θ_0		$a = 0.02$ m^{-1}	0.05	0.1	0.2	0.5	1.0
0°	$b/a = 1$	6.1 ± 0.6 %	11.7	22.0	35.8	55.5	69.5 ± 1.4
	2	6.0 ± 0.7	11.1	20.8	33.3	49.3	58.1 ± 1.0
	4	5.9 ± 0.8	11.0	18.0	26.3	37.3	43.0 ± 0.5
10°	$b/a = 1$	3.2 ± 0.3	7.6	13.1	21.6	39.9	53.6 ± 0.5
	2	3.2 ± 0.2	6.9	12.3	20.4	35.0	46.5 ± 0.4
	4	2.6 ± 0.3	6.4	11.0	17.7	28.6	36.8 ± 0.3
20°	$b/a = 1$	0.6 ± 0.2	2.0	4.4	8.2	17.4	29.8 ± 0.4
	2	0.9 ± 0.2	2.2	4.1	7.6	17.3	28.8 ± 0.4
	4	1.0 ± 0.3	2.0	4.3	7.7	16.4	26.3 ± 0.2
30°	$b/a = 2$	0.5 ± 0.1	1.2	2.2	4.9	11.3	20.9 ± 0.2
40°	$b/a = 2$	0.5 ± 0.1	0.7	1.8	3.5	8.8	16.4 ± 0.1
50°	$b/a = 2$	0.1 ± 0.1	0.6	1.1	2.8	6.9	13.9 ± 0.1
60°	$b/a = 2$	0.2 ± 0.1	0.6	1.0	2.4	6.1	12.1 ± 0.1
70°	$b/a = 2$	0.0 ± 0.1	0.7	1.1	2.3	5.3	11.2 ± 0.2
diffuse	$b/a = 1$	0.5 ± 0.1	1.3	2.6	5.1	11.4	20.0 ± 0.2
	2	0.6 ± 0.1	1.4	2.5	4.9	10.9	19.4 ± 0.2
	4	0.5 ± 0.1	1.5	2.4	4.7	10.2	18.4 ± 0.1

bending nearby incident light in toward the sensor. However, we found this effect to be insignificantly small. Apparently, some photons are refracted toward the shaded region and some are refracted away, giving little overall effect.

In general the upwelling radiance measurement is composed of light that is scattered by the water column into the sensor field of view and of light that is reflected off the seafloor. The former dominates in deep waters with highly absorbing seafloors and the latter dominates in shallow waters with highly reflective bottoms. The shading error in the water column component is approximately that given in Table 1 for large depths, but increases as the water depth is decreased. The component of the radiance measurement due to reflectance off the bottom also contains some shading error because the TSRB casts a shadow on the bottom that will always be at least partially in the field of view of the radiance sensor. However, we found that usually, but not always, the shading error of the bottom component is smaller than that for the water column. Therefore, for shallow waters and highly reflecting bottoms, where the bottom signal dominates over the water column signal, the overall shading error is often much smaller than in optically deep water with the same water properties. For example, Fig. 6 shows the shading error as a function of total water depth for the case of $a = 0.2$ m^{-1}, $b = 0.4$ m^{-1}, and bottom irradiance reflectance $R_b = 0.2$. In very shallow water the radiance measurement is dominated by the component of light being reflected off the bottom. As the depth is increased, the shading error in the radiance reflected off the bottom decreases, as does the overall shading error. However, as the water depth is further increased beyond 4 m, the water-column component of the upwelling radiance begins to dominate and the overall shading error increases toward the optically deep values.

4 Discussion

The self-shading of in-water light-measuring instruments depends on the illumination conditions, water depth, and water and seafloor optical properties. The shading of sea-

#32933 - $15.00 US Received April 17, 2001; Revised May 01, 2001

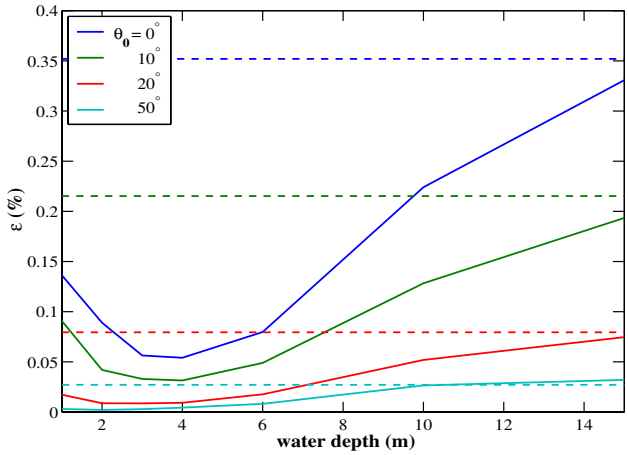

Fig. 6. TSRB self-shading error as a function of water depth for absorption coefficient $a = 0.2$ m^{-1}, scattering coefficient $b = 0.4$ m^{-1}, and bottom albedo $R_b = 0.2$. The dashed lines show the shading error in optically deep waters for solar zenith angles $\theta_0 = 0°$, $10°$, and $20°$.

surface upwelling radiance and irradiance measurements made with cylindrical instruments in optically deep water can be estimated with Eq. (1). However, for other configurations and environmental conditions an empirical approach is required. From three-dimensional Monte Carlo simulations we found that the total shading error of a buoyed instrument in optically-deep water lies between that predicted by Eq. (1) for the radius of the instrument body and that predicted by Eq. (1) for the buoy radius. The error is closer to the former in turbid waters and closer to the latter in clear waters. Because the shading error is greatest at small solar zenith angles, upwelling radiance measurements should be taken when the solar zenith angle is greater than 20°, if possible.

Upwelling radiance measurements obtained with a buoyed instrument should be corrected with data similar to that presented in Table 1. The following steps can be used to apply this correction:

1. Determine the value of $a(\lambda)$ for each radiance wavelength λ. Ideally $a(\lambda)$ is measured from water samples [19, 20] or with an ac-9 (WET Labs, Inc., Philomath, Oregon). Otherwise, given upward and downward irradiance measurements $E_u(\lambda)$ and $E_d(\lambda)$ at two or more depths near the surface, $a(\lambda)$ can be estimated with, for example [21],
$$a(\lambda) = \frac{K_d(\lambda)[1 - R(\lambda)]\cos\theta_0}{0.6 + [0.47 + 2.5R(\lambda)]\cos\theta_0}, \tag{10}$$
where $R = E_u/E_d$ and K_d =-d(log(E_d))/dz. Alternately, given values of $L_u(\lambda)$ at more than one depth, a can be estimated with [7] $a(\lambda) = \chi K_L(\lambda)$, where K_L =-d(log(L_u))/dz and χ is a constant of proportionality valid for the local region. Given $a(\lambda)$ at several wavelengths, $a(\lambda)$ can be modeled for all wavelengths with a bio-optical model [12]. In the absence of any ancillary data, use an $a(\lambda)$ that is at least as large as the published value for pure seawater [12, 22].

2. Estimate $b(\lambda)$ for each wavelength. This is only important if $a(\lambda)$ is large and θ_0 is small. Otherwise, let $b(\lambda) = 2a(\lambda)$. Pure water values of b are given in Refs. 12, 22, and 23, and bio-optical models for $b(\lambda)$ are given in Ref. 12.

3. Given $a(\lambda)$ and $b(\lambda)$, interpolate Table 1 to obtain $\varepsilon_{\rm sun}(\lambda)$ for the appropriate sun zenith angle θ_0. Also interpolate the "diffuse" portion of Table 1 to obtain $\varepsilon_{\rm sky}(\lambda)$.

#32933 - $15.00 US
Received April 17, 2001; Revised May 01, 2001

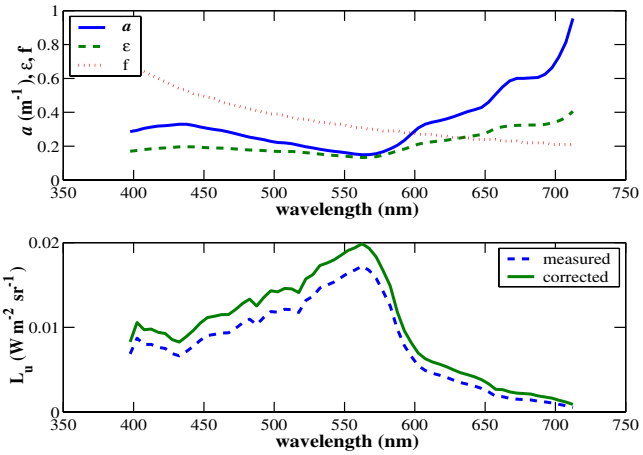

Fig. 7. Example TSRB shading correction. The upper plot shows the water absorption spectrum $a(\lambda)$, the ratio $f(\lambda)$ of skylight to sunlight, and the corresponding shading error $\varepsilon(\lambda)$. The lower plot shows the measured and corrected upwelling radiance spectra.

4. For each wavelength determine the ratio of skylight to direct sunlight, $f(\lambda)$. This can be done from direct measurement (e.g., with a sun photometer), with an empirical atmospheric model [18, 24], with the procedure given by Gordon [25], or by selecting published values [26].

5. Determine the total shading error $\varepsilon(\lambda)$ for each wavelength with Eq. (2).

6. Compute the true radiance spectrum $L_u^{\text{true}}(\lambda)$ from the measured radiance $L_u^{\text{m}}(\lambda)$ with

$$L_u^{\text{true}}(\lambda) = L_u^{\text{m}}(\lambda)/(1 - \varepsilon(\lambda)). \tag{11}$$

An example TSRB shading correction is demonstrated in Fig. 7. The water absorption spectrum shown in the upper plot is typical of case I waters with relatively high chlorophyll concentration (10 mg/m) [12]. The measured radiance spectrum shown in the lower plot is for a solar zenith angle of 10° and a sky with 20% clouds. The ratio of skylight to sunlight $f(\lambda)$ shown in the upper plot was computed using an empirical atmospheric model [24]. The corresponding shading error $\varepsilon(\lambda)$ was determined with Table 1 and Eq. (2) and was applied to the measured radiance spectrum to obtain the corrected radiance spectrum shown in the lower plot.

A Fortran routine that replaces steps 3–5 above is available from the authors. This routine uses neither Table 1 nor Eq. (2), but instead applies modeled sky conditions to tabulated values of BMC ray-tracing statistics. It is important to note that the shading error values given in Table 1 are only valid for optically deep water, calm sea-surface conditions, and particular TSRB dimensions. Different tables need to be used for different situations. Although it is not practical to provide many tables here, the shading error for many different water depths, bottom types, and sea surface roughness are being compiled for use in the Fortran routine.

Acknowledgments

This work was supported by the U.S. Office of Naval Research. Author C.D.M. was supported by ONR's Environmental Optics Program. We thank Marcos Montes for his helpful suggestions.

#32933 - $15.00 US
Received April 17, 2001; Revised May 01, 2001